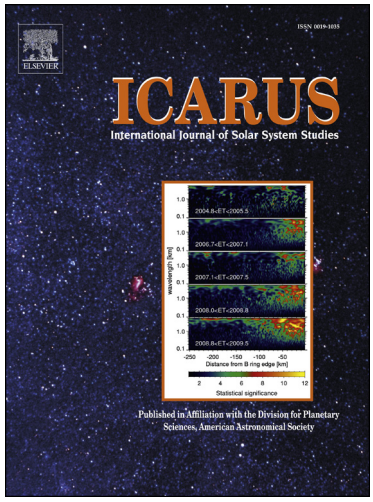

Cellinoid Shape Model for Hipparcos Data

Xiao-Ping Lu, Alberto Cellino, Daniel Hestroffer, Wing-Huen Ip

PII: S0019-1035(15)00556-4
DOI: http://dx.doi.org/10.1016/j.icarus.2015.12.006
Reference: YICAR 11827

To appear in: *Icarus*

Received Date: 5 May 2015
Revised Date: 12 November 2015
Accepted Date: 5 December 2015

Please cite this article as: Lu, X-P., Cellino, A., Hestroffer, D., Ip, W-H., Cellinoid Shape Model for Hipparcos Data, *Icarus* (2015), doi: http://dx.doi.org/10.1016/j.icarus.2015.12.006

Cellinoid Shape Model for Hipparcos Data

Xiao-Ping Lu[a,b], Alberto Cellino[c], Daniel Hestro er[d], Wing-Huen Ip[b,e]

[a] *Faculty of Information Technology, Macau University of Science and Technology, Macau, China*
[b] *Space Science Institute, Macau University of Science and Technology, Macau, China*
[c] *INAF, Astronomical Observatory of Torino, strada Osservatorio 20, 10025 Pino, Torinese, Italy*
[d] *IMCCE, Observatoire de Paris, 77 Av. Denfert Rochereau, 75014 Paris, France*
[e] *Institute of Astronomy, National Central University, Taiwan*

Abstract

Being intermediate between a regular triaxial ellipsoid shape and a more complex convex shape, the so-called "cellinoid" shape model consists of eight octants of eight ellipsoids with the constraint that neighbouring octants share two common axes. The resulting variety of possible shapes, obtained at the cost of only three extra parameters to be added to models of regular ellipsoids, can be employed to e ciently simulate asteroids with irregular shapes. This article shows how the cellinoid shape model can be applied to the inversion of sparse photometric data, such as Hipparcos data. In order to make the model more e cient and convenient to use, an error analysis is discussed and numerically confirmed. Finally, we determine physical parameters of several asteroids, including their shape, rotational period and pole orientation, by applying our model to Hipparcos data.

Keywords: Asteroids, Photometry, Sparse data, Shape model, Hipparcos data
2010 MSC: 00-01, 99-00

1. Introduction

A statistical analysis of the main physical parameters of asteroids, including their shape and spin properties, is important in order to shed some light on the early phases of formation of the solar system, as well as its subsequent evolution. Generally, the primary data source for deriving these parameters is the analysis of lightcurves obtained

Corresponding author
Email address: (Xiao-Ping Lu)

via ground-based telescopes. However, among the more than 600,000 asteroids discovered so far, less than 3,000 of them have at least one lightcurve (Warner et al., 2009). Fortunately, there are several large sky survey projects, both past and present, that have obtained photometric observations of asteroids from the ground and from space. Gaia, launched at the end of 2013, is a large mission whose aim is to chart a three dimensional map of our galaxy. It is observing and recording the positions of hundreds of thousands of stars, as well as obtaining highly accurate photometric data of the bodies within the solar system, primarily asteroids (Jordi et al., 2010; Cellino and Dell'Oro, 2012). Unlike classical lightcurves, the photometric data collected of asteroids by satellites are sparse. For every asteroid observed in the main belt, there may be about 70 photometric snapshots in total. The problem of deriving spin and shape parameters from these sparse data are not trivial. In this article, we present a detailed technique and search strategy to make the cellinoid shape model stable and e cient when deriving these parameters. As Gaia is currently collecting data, which are not yet publically available, HIPPARCOS (HIgh-Precision PARallax COllecting Satellite) data are used instead in our analysis to test the algorithm. Hipparcos was a satellite launched by ESA, the European Space Agency, in 1989, which collected some sparse photometric data for a small number of asteroids. Gaia was conceived to dramatically increase and improve the results of Hipparcos both in measured precision and the number of targets observed.

In the past, the methods that were used to derive asteroid shapes from photometric data were based on polyhedron models of regular triaxial ellipsoids (Surdej and Surdej, 1978). Karttunen (1989) presented a method for modelling asteroid brightness variation based on a triaxial ellipsoid shape, and he also discussed and modelled spherical concavities to mimic macroscopic shadowing and albedo. Additionally, Karttunen and Bowell (1989) discussed the influences of scattering, and concluded that lightcurves amplitudes depend very strongly on body shape. This was then confirmed by Cellino et al. (1989). Ohba et al. (2003) analysed pole orientation based on a triaxial ellipsoid shape for the target asteroid of the MUSES-C mission, (25143) 1998 SF36. Drummond et al. (2010) employed the ellipsoid model to estimate the physical properties of the ESA Rosetta target asteroid (21) Lutetia, such as its dimensions, rotational pole and bulk

density. Cellino et al. (2009) applied the ellipsoid model to Hipparcos data using a genetic inversion method, and showed that sparse photometric data could also be exploited when estimating the physical parameters of asteroids. Lu et al. (2013) introduced a numerical algorithm based on the ellipsoid model to e ciently calculate the rotational periods and pole orientations of asteroids.

The regular triaxial ellipsoid model, which has three parameters, is simple but e - cient when applied to the task of simulating asteroid shapes. However, due to the symmetric structure of the ellipsoid, it has a limited capability for determining the photometric variation of objects that possess more complex shapes. Kaasalainen and Lamberg (1992a,b) presented a method to simulate complex asteroid shapes using a convex polyhedron representation. They used the Gaussian curvature function to describe the surface of an asteroid via spherical harmonics, instead of its radial function, which made the algorithm numerically stable and the solutions were seen to converge. The very good performances of this model were proven through applications to the cases of several asteroids for which several lightcurves are available (Kaasalainen and Torppa, 2001; Kaasalainen et al., 2001). Furthermore, Kaasalainen et al. (2012) made the method more e cient by employing Lebedev quadrature to calculate the surface integration. Kaasalainen's method performs very well when simulating asteroids with irregular shapes, as also confirmed by laboratory experiments (Kaasalainen et al., 2005).

As described previously, the simple triaxial ellipsoid can e ciently derive approximate, but generally acceptable, solutions to the physical parameters of asteroids(Santana-Ros et al., 2015), while the convex model can derive more accurate estimates from many lightcurves that cover a wide range of observing geometries. Commonly we have at our disposal for some objects either several lightcurves taken at just one apparition, or sets of sparse photometric snapshots taken at various epochs by sky surveys. This is the main reason why the ellipsoid shape model has been employed very frequently until now. However, the symmetric shape of a triaxial ellipsoid has some limitations when used to simulate the irregular shapes of many asteroids. Cellino et al. (1989) presented a definition of the shape model, which consisted of eight octants from eight ellipsoids with the constraint of neighbouring octants sharing the same two semi-axes. Based on this shape, it is possible to simulate the behaviour of a large variety of convex and complex shapes.

Lu et al. (2014) firstly called the shape 'cellinoid' and presented a theoretical method to derive physical parameters from lightcurves based on the cellinoid model. Furthermore, Lu and Ip (2015) introduced a technique that reduces lightcurves to make the method more e cient, and applied the cellinoid shape model to multiple lightcurves observed in various geometries. The cellinoid shape model includes three more parameters than the regular triaxial ellipsoid shape model, and can be employed to simulate the asymmetric shape structure of irregular asteroids. The computational cost is not increased hugely, while the accuracy of derived physical parameters from several lightcurves is higher than the ellipsoid model (Lu et al., 2014). Moreover, the shape and the physical parameters could be refined by using more lightcurves observed in various geometries (Lu and Ip, 2015).

This article focuses on the application of the cellinoid shape model to sparse datasets, such as Hipparcos data. As the photometric data are sparse, the whole inverse process is di erent to the ones employed for lightcurves, and the detailed technique and search strategy are introduced. Additionally, as the number of the sparse data are limited, the error propagation is analyzed carefully. In this article, the whole cellinoid shape model for sparse datasets are presented in Section 2 and the theoretical analysis for its error propagation is discussed in Section 3. Then, the whole process is examined by applying it to a simulated asteroid with the exact cellinoid shape in Section 4. Finally, the cellinoid shape model for sparse datasets are applied to the Hipparcos data in Section 5. The resulting physical parameters for some asteroids are listed and compared with known results obtained from other methods. At the end, the conclusion is presented and future work is discussed.

2. Cellinoid Shape Model

2.1. Cellinoid Shape

With six semi-axes a_1 a_2 b_1 b_2 c_1 c_2, the cellinoid shape model is defined in Fig.(1).

The volume of the cellinoid shape is

$$M \quad \frac{}{6}(a_1 \quad a_2)(b_1 \quad b_2)(c_1 \quad c_2) \tag{1}$$

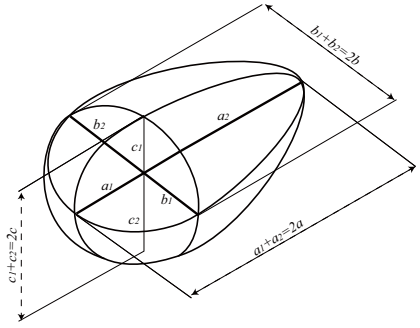

Figure 1: Cellinoid shape model

and its centre is

$$G \quad \begin{matrix} \bar{x} & \frac{3}{8}(a_1 \quad a_2) \\ \bar{y} & \frac{3}{8}(b_1 \quad b_2) \\ \bar{z} & \frac{3}{8}(c_1 \quad c_2) \end{matrix} \tag{2}$$

As the cellinoid shape model is asymmetric, its centre varies with respect to the semi-axes. Moreover, its free rotational axis is not the z-coordinate axis, as in the case of an ellipsoid. As described by Lu and Ip (2015), the free rotational axis can be derived by diagonalizing the matrix $C \quad A \quad M \quad B$, where the definitions of A, and B are as follows,

$$A \quad \begin{matrix} I_{xx} & I_{xy} & I_{xz} \\ I_{xy} & I_{yy} & I_{yz} \\ I_{xz} & I_{yz} & I_{zz} \end{matrix} \tag{3}$$

$$B \quad \begin{matrix} \bar{y}^2 & \bar{z}^2 & \bar{x}\bar{y} & \bar{x}\bar{z} \\ \bar{x}\bar{y} & \bar{x}^2 & \bar{y}^2 & \bar{y}\bar{z} \\ \bar{x}\bar{z} & \bar{y}\bar{z} & \bar{x}^2 & \bar{y}^2 \end{matrix} \tag{4}$$

The elements in A have the similar forms, such as

$$I_{xx} \quad (y^2 \quad z^2)dV \quad \frac{}{30}(a_1 \quad a_2)(b_1^3 \quad b_2^3)(c_1 \quad c_2) \quad (a_1 \quad a_2)(b_1 \quad b_2)(c_1^3 \quad c_2^3)$$

$$I_{xy} \quad (xy)dV \quad \frac{1}{15}(a_1^2 \quad a_2^2)(b_1^2 \quad b_2^2)(c_1 \quad c_2)$$

2.2. Scattering Law

Muinonen et al. (2002) introduced a joint linear-exponential model

$$f(\ ) \qquad \exp(\ -) \tag{5}$$

to simulate the photometric phase curve, where is the solar phase angle and and are three linear parameters, while is a nonlinear parameter. As the solar phase angle approaches 0, i.e. corresponding to ideal solar opposition, the model can provide a good simulation of real observations. Combing the phase curve function, Kaasalainen et al. (2001) presented a scattering function

$$S(\ _0\ )\ \ f(\ )\ \frac{\ \ 0}{\ \ 0}\ \ _0 \tag{6}$$

with a weight factor , where and $_0$ are the projections of the viewing unit vector (the Earth direction) and illuminating unit vector (the Sun direction) on the normal direction of the asteroidal surface. (In other words, and $_0$ are the cosines of the emergence angle and of the incidence angle, respectively).

The Hipparcos mission collected photometry of some asteroids from 1989 to 1993 (Perryman et al., 1997; Hestro er et al., 1998). Di erent to ground-based observations, Hipparcos photometric data are sparse and are not continuous. Generally, the number of points for most of asteroids in Hipparcos data are less than a few tens. Additionally, the Hipparcos photometric data of asteroids also have poor accuracies (Cellino et al., 2009). Therefore, the number of constraints to e ectively simulate the asteroid is limited, which is why the traditional triaxial ellipsoid model is still frequently employed when simulating asteroids. In this article, there are five free parameters when simulating asteroids by the cellinoid shape model, i.e. a_2 b_1 b_2 c_1 and c_2, where we also assume that a_1 1. In addition to the pole direction ( ) in the ecliptic coordinate system, the rotational period P, initial rotational phase angle $_0$, and five scattering parameters ( ), the total number of parameters in the cellinoid shape model is thus 14. It is reasonable to search for the best-fitting parameters by applying the cellinoid shape model to Hipparcos data.

2.3. Inverse Process

With the definition of the scattering law in Eq.(6), the observed brightness of a given asteroid under a specific viewing geometry, i.e. the position of the Earth and the Sun, can be computed by the surface integration,

$$L(\quad _0) \qquad _C \; S(\quad _0 \quad) \, ds \tag{7}$$

where C is the part of the surface of the cellinoid shape model, both illuminated and viewed, i.e. 0, and $_0$ 0.

As the Hipparcos data are sparse, the ^{2} should be defined with the standard deviation $_i$ of each data point as follows,

$$^2 \qquad _i \; \frac{L_i \quad \hat{L}_i}{_i} \; ^2 \tag{8}$$

where L_i is the brightness of the i-th observed point, while $\hat{L}_i$ is the i-th corresponding fitted brightness. Then some optimization tools, such as the genetic algorithm, or Levenberg-Marquardt algorithm, can be employed to search for the best-fitting solutions that minimize ^{2}.

3. Error Propagation and Constraints

As the sparse data for constraining the physical parameters of the cellinoid shape model are inaccurate, the error propagation of the volume, centre of the cellinoid shape, and free rotational axis with respect to the six semi-axes must be considered. Besides, some constraints need to be applied to make the whole algorithm more robust.

3.1. Error Propagation

The error propagation is linear for the centre of the cellinoid shape in Eq.(2) with respect to the six semi-axes a_1 a_2 b_1 b_2 c_1 and c_2. Furthermore, the volume in Eq.(1) increases as k^3 as the semi-axes increases with k to the power of three, which will make the algorithm unstable if the semi-axes substantially increase. Generally, we add the constraint of fixing a_1 to 1, and the other semi-axes will be adjusted proportionally.

The free rotational axis is complicated to derive by calculating the eigen-decomposition of the matrix C. Since the matrices A B in Eqs.(3,4) are real symmetric, the eigenvalues are real and the eigenvectors are orthogonal. For simplicity, the matrix C can be simplified to $C \quad (a_1 \quad a_2)(b_1 \quad b_2)(c_1 \quad c_2)F$, with the definition of a real symmetric 3 3 matrix F as follows,

$$
\begin{aligned}
F_{11} \quad & \frac{19}{1920}b_1^2 \quad \frac{19}{1920}b_2^2 \quad \frac{13}{960}b_1b_2 \quad \frac{19}{1920}c_1^2 \quad \frac{19}{1920}c_2^2 \quad \frac{13}{960}c_1c_2 \\
F_{22} \quad & \frac{19}{1920}a_1^2 \quad \frac{19}{1920}a_2^2 \quad \frac{13}{960}a_1a_2 \quad \frac{19}{1920}c_1^2 \quad \frac{19}{1920}c_2^2 \quad \frac{13}{960}c_1c_2 \\
F_{33} \quad & \frac{19}{1920}a_1^2 \quad \frac{19}{1920}a_2^2 \quad \frac{13}{960}a_1a_2 \quad \frac{19}{1920}b_1^2 \quad \frac{19}{1920}b_2^2 \quad \frac{13}{960}b_1b_2 \\
F_{12} \quad F_{21} \quad & (\frac{3}{128} \quad \frac{1}{15})(a_1 \quad a_2)(b_1 \quad b_2) \\
F_{13} \quad F_{31} \quad & (\frac{3}{128} \quad \frac{1}{15})(a_1 \quad a_2)(c_1 \quad c_2) \\
F_{23} \quad F_{32} \quad & (\frac{3}{128} \quad \frac{1}{15})(b_1 \quad b_2)(c_1 \quad c_2)
\end{aligned}
$$

The eigen-decomposition of C can be calculated simply from the eigen-decomposition of F with the same eigenvectors, where the proportional eigenvalues increase by a factor of $(a_1 \quad a_2)(b_1 \quad b_2)(c_1 \quad c_2)$. Let the eigenvectors of matrices C and F be $[v_1 \; v_2 \; v_3]$ with respect to the three eigenvalues of the matrix F, $[\ _1 \quad _2 \quad _3]$, which are arranged from the smallest to the largest. To estimate the error propagation in the optimization process of the cellinoid shape model, we performed a numerical test. Given a random set of six semi-axes where the first one is fixed to 1, we calculated the three eigenvectors of the matrix C and a 5% error was added to each semi-axis except for the first fixed one a_1, then the new three eigenvectors of the matrix C were calculated. Comparing the error of the norm of the deviation of two eigenvectors,

$$v_{i\ 2} \quad v_i \quad u_{i\ 2}\ i \quad 1\ 2\ 3$$

in which v_i is the i-th eigenvector of the original matrix and u_i is the i-th eigenvector of the matrix with 5% Gaussian noise added, we repeated the test 10,000 times. The three maxima and the mean of the norm for the three eigenvectors are listed in Table 1 for the five semi-axes, respectively. Intuitively, the max and mean norm of the numerical test for 10,000 simulations are under 5%, which means the eigenvectors of matrix C

converged as the six semi-axes converged. As described previously, the three orthogonal eigenvectors of the matrix C are the three new coordinate axes, and the eigenvector of the largest eigenvalue is the new z-axis, i.e. the free rotational axis of the cellinoid shape model.

Table 1: Numerical Test for Error Propagation of Five Semi-Axes

Semi-Axis	Max Norm: [$v_{1\ 2}$ $v_{2\ 2}$ $v_{3\ 2}$]	Mean Norm: [$v_{1\ 2}$ $v_{2\ 2}$ $v_{3\ 2}$]
a_2	[0.02571, 0.02533, 0.00443]	[0.00161, 0.00125, 0.00073]
b_1	[0.00740, 0.00780, 0.00416]	[0.00101, 0.00149, 0.00086]
b_2	[0.00601, 0.00701, 0.00461]	[0.00053, 0.00152, 0.00131]
c_1	[0.00247, 0.01180, 0.01188]	[0.00027, 0.00082, 0.00092]
c_2	[0.00189, 0.00541, 0.00542]	[0.00012, 0.00032, 0.00037]

3.2. Constraints

As the scattering law in Eq.(5) can adjust the relative brightness of the model, the total brightness of the modelled shape scales with the size. The total parameters used to control the cellinoid shape are reduced to five and the other five semi-axes can be adjusted proportionally. Meanwhile, the parameters and in Eq.(5) can be adjusted to balance the whole brightness integration in Eq.(7).

Since the coordinate system of the asteroid can be selected freely, the constraint

$$a_1 \quad a_2 \quad b_1 \quad b_2 \quad c_1 \quad c_2$$

is added to make the cellinoid similar to the standard ellipsoid, where the three axes a b c. Additionally, we let a_1 a_2 to make the longest axis occur at the positive direction of the x-axis.

In all, the constraints to the six semi-axes are generally set as follows,

(1) a_1 1;

(2) a_1 a_2 b_1 b_2 c_1 c_2;

(3) a_1 a_2.

4. Application to Synthetic Sparse Data

In order to test the stability of the algorithm based on the cellinoid shape model, as described in Section 2.3, the inverse process of constraining the free parameters by minimizing ^{2} in Eq. (8) was first applied to synthetic sparse data. The procedure used to derive the best-fitting results is described in detail as follows.

4.1. Generating Synthetic Sparse Data

The method presented in this article is primarily applied to sparse datasets of asteroids, such as those obtaied by Hipparcos and Gaia. In order to better simulate real observations, synthetic sparse data were generated to match the cadence and photometric uncertainties obtained by Hipparcos. Here we used the asteroid Laetitia (39) as an example to illustrate the whole inversion process. The total number of observations of Laetitia (39) is 112, which is the largest amount obtained for all asteroids recorded by Hipparcos.

First, the related parameters are preset as

$$[1\ 0\,9\ 0\,85\ 0\,7\ 0\,6\ 0\,5\ 43\ 70\ 5\,5\ 100\quad 0\,5\ 1\ 0\,1]$$

following the sequence of six semi-axes (a_1 a_2 b_1 b_2 c_1 and c_2), pole orientation ( ) in the ecliptic coordinate frame, rotational period (P) with the initial rotational phase angle ($_0$), and the three scattering factors ( ) in Eq. (6).

It should be noticed that the other two parameters, and in Eq. (6), are ignored here as the solar phase angles of Laetitia (39) recorded in the Hipparcos data are distributed between 13 62 and 23 62 , with a mean angle of 17 95 , for which the opposition e ect is not relevant.

Second, the brightness of Laetitia (39) in the Hipparcos data is replaced by the synthetic brightness calculated via Eq. (7) using the preset parameters and the corresponding observed geometries of Laetitia (39).

Then, the generated synthetic sparse data were used to verify the cellinoid shape model. Furthermore, in order to better simulate real observations, we also applied the shape model to the noised synthetic sparse data. Gaussian noise with a mean value of

0 mag and a standard deviation of 0 01 mag were added to the previously generated sparse data.

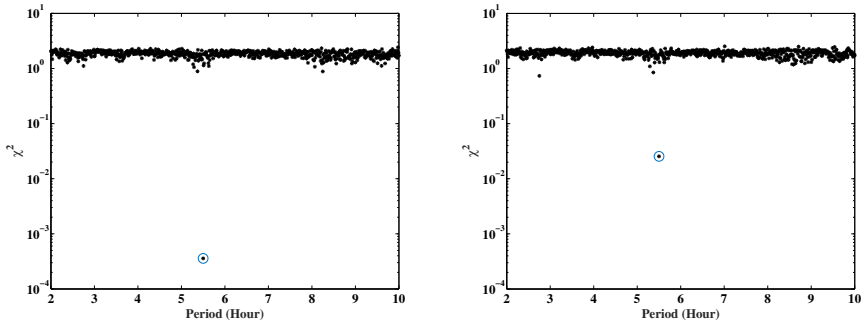

Figure 2: Searching for the best-fit period(circled point) from synthetic sparse data based on Laetitia (39). Synthetic sparse data without adding Gaussian noise(Left), synthetic sparse data adding Gaussian noise(Right)

4.2. Searching for the Best-fitting Period

The generated synthetic sparse data with the given parameters were treated as real observed sparse data. The caveat here of course is that its shape is that of an ideal cellinoid and not the complex shape of a real asteroid. The most important thing when deriving the fitted parameters by the cellinoid shape model is to search for the best-fit period correctly. For most situations, the periods are unknown, especially for newly found asteroids. Fortunately, as described by Warner et al. (2009), most asteroids have rotational periods that are greater than about 2.2 hours with the majority being between four and 10 hours. Based on that, if we do not have any prior information of a given asteroid, a first-approximation search with a test period ranging from two to 10 hours is implemented. However, for some special asteroids if the ^{2} of the derived best-fit period is not enough small, the period search should be enlarged to the interval 10 to 20 hours.

Fig. 2 presents the distribution of ^{2} for di erent test periods for both the synthetic sparse data and the synthetic sparse data with added Gaussian noise. It should be

noticed that ^{2} in Eq. (8) would be modified to

$$^2 \quad _i \quad L_i \quad \hat{L}_i \; ^2 \tag{9}$$

for the synthetic sparse data without Gaussian noise as its standard error is zero. As shown in Fig. 2, the inversion process can correctly derive the initial period of both the sparse data and the noised sparse data. The circled points in Fig. 2 are the derived best-fitting periods. The ^{2} of best-fitting period for the noised synthetic sparse data is higher than that of the non-noised sparse data, but it is good enough to distinguish from the other test values of the period.

It is a time-consuming process to search for the best-fitting period. Kaasalainen et al. (2001) presented a strategy to search for the best-fitting period for events where the obtained lightcurves span many years and apparitions because the period space is filled with densely packed local minima. The smallest separation P of the local minima when searching the period should roughly be given by

$$\frac{P}{P} \quad \frac{1}{2}\frac{P}{T} \tag{10}$$

where $T \quad \max(t \quad t_0)$ within a lightcurve set. In our test of the synthetic sparse data based on Laetitia (39), as the observed period is $T \quad 966\ 32 days$, the corresponding separation P should be $0\ 000086h$ for $P \quad 2h$, and $0\ 0022h$ for $P \quad 10h$.

However, in the real implementations, $P \quad 0\ 01h$ was enough for the synthetic sparse data. If there was some prior information about the period of the asteroid, the search interval could be reduced to save computing time.

4.3. Searching for the Best-fitting Pole and Shape

With the derived best-fitting period, we searched for the pole orientation with a resolution of 3 on the unit sphere. There were a total of 7320 tests. For each test, the period and pole orientation were specified, while the other parameters could be chosen freely. Then, the Levenberg-Marquardt algorithm was employed to search for local optimal solutions with the initially specified parameters. All of the derived locally optimal pole orientations are shown in Fig. 3, denoted by the grey points.

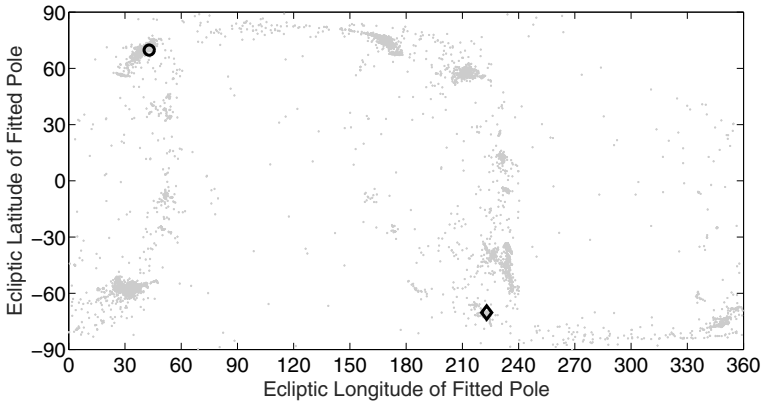

Figure 3: Searching for the best-fit pole orientation (big circle) and accompanying solution (big diamond) from synthetic sparse data based on Laetitia (39).

As the synthetic sparse data were generated with a specific cellinoid shape, and the brightness was also calculated via the same algorithm in Eq. (7) in the inversion process, the preset solutions could be searched by the optimization algorithm. The derived best-fitting solution with ^{2} 10 ^{29} is the same as the preset one,

[1 0 9 0 85 0 7 0 6 0 5 43 70 5 5 100 0 5 1 0 1]

Furthermore, we found that all 37 of the best-fitting solutions with ^{2} less were than 10 ^{25}, in which there were 32 solutions with a pole orientation of (43 70) denoted by a big circle in Fig. 3, and five solutions with a pole orientation of (223 70), denoted by a big diamond in the same figure. The solutions with the pole (43 70) are the same as the preset one, while the solutions with the pole (223 70) are di erent. For example, one solution is,

[1 0 8235 1 0588 1 1765 0 7059 0 5882 223 70 5 5 100 0 3613 0 7226 0 1]

However, if the six semi-axes are divided by the largest semi axis, the six semi-axes

would be

[0 8500 0 7000 0 9000 1 0000 0 6000 0 5000]

which is the same as the preset one, although the sequence changes. Similarly, the first two scattering factors of this solution are also proportional to the preset ones.

As the cellinoid shape is asymmetric, one can use the shape model to adjust the semi-axes, the initial phase angle, and scattering factors to fit the reverse direction of the pole (43 70). That is why we added the constraints to the six semi-axes in Sec. 3.2. Nevertheless, this is also a very good phenomenon for the whole inversion process to confirm the correct pole orientation, i.e. the pole search can derive the correct pole orientation, accompanying a reverse one if we do not constrain the semi-axes.

Following the previous process, the pole search was also applied to the noised synthetic sparse data. The derived pole orientation is (42 5 69 6) with the ^{2} 0 0383 and the six semi-axes are

[1 0 8860 0 8584 0 7171 0 6749 0 4103]

Although the derived semi-axes c_1 c_2 are not very close to the preset c_1 0 6 c_2 0 5, the mean value 0 5426 of c_1 and c_2 is close to the mean value 0 55 of preset c_1 and c_2.

Analogously, the pole search also derives another pole orientation (222 5 69 5).

Besides, we also performed the numerical tests in the same way based on the other asteroids. All of the best-fitting results are similar to the initial ones. For example, Fig. 4 shows that the period search for both synthetic sparse data and noised synthetic sparse data based on the asteroid Hebe (6). The initial related parameters are

[1 0 85 0 75 0 6 0 5 0 7 143 50 6 5 140 0 6 1 2 0 4]

The circled points in Fig. 4 are the best-fitting periods, which are close to the initial one, P 6 5 hr.

As shown in Fig. 5, for the synthetic sparse data with added Gaussian noise, the pole search derived the best-fitting pole orientation (141 8 51 5) with the six semi-axes,

[1 0 8934 0 7690 0 6137 0 4868 0 7248]

And the other accompanying pole orientation was (321 8 51 5).

The numerical simulations confirmed that the cellinoid shape model is self-consistent, and the period search could derive a best-fitting result whose value was close to the pre-set one. Then the pole search could subsequently derive the correct pole orientation. It should be noted that the reverse pole orientation would emerge as an accompanying result, whose semi-axes and scattering factors would change proportionally. Besides, there is no need to search for the best-fitting shape again, as the pole search for the 7320 initial tests could cover enough test values of the semi-axes, and the Levenberg-Marquardt algorithm could e ciently search for the locally optimal solution.

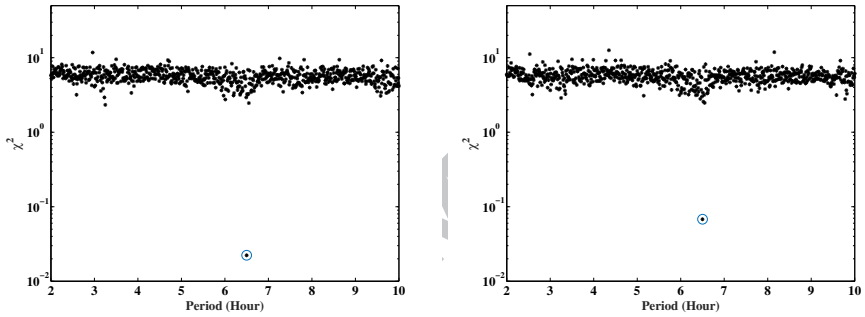

Figure 4: Searching the best-fit period (circled point) from synthetic sparse data based on Hebe (6). Synthetic sparse data without adding Gaussian noise(Left), synthetic sparse data with adding Gaussian noise(Right)

5. Application to Hipparcos Data

Following the successful strategy applied in the synthetic sparse data, the cellinoid shape model was employed to Hipparcos data. Again, we used the asteroid Laetitia (39) as an example to show the whole process of searching for the related physical parameters of the asteroid from the sparse data, and make a comparison with known solutions obtained via other methods and authors.

As illustrated previously, the better search scheme for the period is to search the interval from 2 hours to 10 hours with a separation P 0 000086h. However, this will be a very time-consuming task. In real implementations to Hipparcos data, we searched the interval [2 10] with an increment of P 0 005h for the first rough

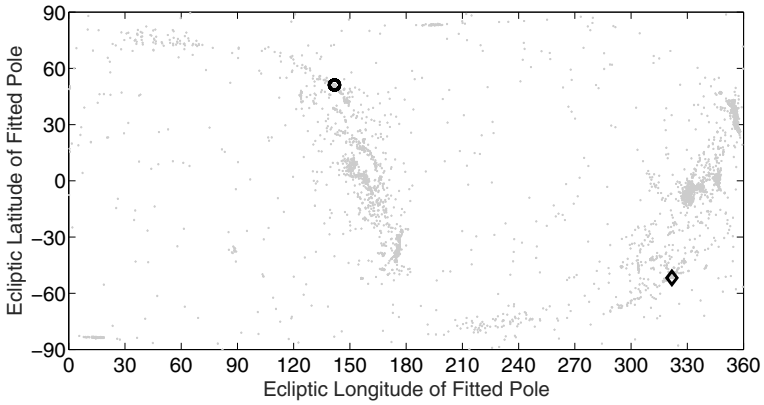

Figure 5: Searching the best-fit pole orientation (big circle) and accompanying solution(big diamond) from synthetic sparse data based on Hebe (6).

search, as shown in Fig. 6(a). The derived best-fitting period of asteroid Laetitia (39) is P 5 21h. Moreover, in Fig. 6(a) there are also some other possible period solutions derived at local minima, where the ^{2} of the period was smaller than ones of neighbouring periods. Therefore, we manually add these possible period solutions into the interval [3 4 3 6 5 1 5 3 7 3 7 4 9 7 9 8] to a refined search with an increment of P 0 001h, as shown in Fig. 6(b). Then a best-fitting period of P 5 17h was derived. Finally, we searched the interval from 5 1 hours to 5 2 hours with an increment of P 0 0001h, as shown in Fig. 6(c). The derived best-fitting period was P 5 138h. The search for the period in this way could save much computational time.

With the derived best-fitting period, a pole search was implemented. The derived local optimal pole orientations are shown in Fig. 7. The pole orientation with the smallest ^{2} is (313 4), denoted by the big circle in Fig. 7, while the corresponding accompanying pole solution is (133 4), denoted by the big diamond in Fig. 7. The

derived semi-axes of the shape are

$$a_1 \quad 1 \; a_2 \quad 0\,65 \; b_1 \quad 0\,74 \; b_2 \quad 0\,43 \; c_1 \quad 0\,62 \; c_2 \quad 0\,43$$

and the refined period is $P \quad 5\,13830h$ with the three scattering parameters $3\,6 \quad 5\,5 \quad 0\,23$.

As the observing error could a ect the solutions, and the scattering law cannot accurately simulate the real situation, here we show the distribution of the possible pole results with the 300 smallest ^{2} in Fig. 8 and present a second possible pole solution for reference. The results can be classified into two groups. Generally, the deviations of both the longitude and latitude of the similar pole solutions classified in the same group are less than 3 . The first is the one with the smallest ^{2}, (313 4), denoted by the big circle, where its accompanying pole (133 4) is denoted by the big diamond. The second is (318 23), denoted by the upward triangle, and its accompanying pole (138 23), is denoted by the downward triangle in Fig. 8. The corresponding period of the second group of the pole orientation is $P \quad 5\,13827h$, and its six semi-axes are

$$a_1 \quad 1 \; a_2 \quad 0\,61 \; b_1 \quad 0\,67 \; b_2 \quad 0\,51 \; c_1 \quad 0\,57 \; c_2 \quad 0\,45$$

Based on the cellinoid shape model, the derived rotational period of Laetitia (39) from the Hipparcos data is consistent with the known results, such as Kaasalainen's method (Kaasalainen et al., 2002; Ďurech et al., 2011; Hanuš et al., 2013) and the inversion method (Cellino et al., 2009), shown in Tab. 2. Besides, as we have derived two possible pole orientations due to the limited data source, the second pole (318 23) is close to the pole solution (323 32) determined via Kaasalainen's method with the longitude deviation 5 and the latitude deviation 9 , which is based on 56 lightcurves obtained from 1949 to 1988. The accompanying direction (133 4) of the first pole result is similar to the second result (126 20) obtained by Cellino, with a longitude deviation 7 and a latitude deviation 16 , who derived the pole solution based on the same data source. Therefore, from only 112 observed snapshots of Laetitia(39) in the Hipparcos data, the cellinoid shape model could derive the rotational period and provide a reasonable estimate of the pole orientation. Furthermore, the cellinoid shape model could present a rough profile of the asteroid from the sparse dataset; this is in

contrast to the convex shape model, which requires many lightcurves to reconstruct its surface and which has more than 50 parameters.

Generally speaking, the process of searching for the physical parameters of asteroids from sparse photometric data based on the cellinoid shape model could be split into four steps. First, a rough estimate of the period is derived by searching the period interval [2, 10] with a separation of P 0 005h. Second, a refined estimate of the period is derived by searching the period interval that covers the local minima in the first rough period search with a separation of P 0 001h. Third, the best-fitting period will be derived by searching the period interval covering the absolute minimum in the second period search with a separation of P 0 0001h. Fourth, with the derived best-fitting period a pole search is implemented on the unit sphere with a resolution of 3 . The pole solution with the least ^{2} is taken as the best-fitting pole value. Meanwhile, the cellinoid shape model that corresponds to the best-fitting pole value is derived.

Applying the same process based on the cellinoid shape model to other asteroids recorded in Hipparcos data, the best-fitting parameters were derived and are listed in the final column of Tab. 2. The first column lists the names and numbers of asteroids with their total numbers of observations by Hipparcos. For comparison, the known results from other methods are also listed respectively in the second and third columns, including the results in DAMIT by Kaasalainen's method (Ďurech et al., 2010) and the inversion solutions based on the triaxial ellipsoid shape model by Cellino et al. (2009). In the following subsections, we will present the details for each individual asteroid.

5.1. Hebe (6)

There are a total of 91 observed snapshots in the Hipparcos data. The solar phase angles are between 14 94 and 30 59 with a mean value of 20 30 . The derived rotational period determined by the cellinoid shape model is P 7 27806h, and the best-fitting pole orientation is (342 39) with a longitude deviation of 2 and a latitude deviation of 3 to the result Pole$_1$(340 42) by Kaasalainen's method (Torppa et al., 2003; Ďurech et al., 2011). The derived six semi-axes are

$$a_1 \quad 1 \;\; a_2 \quad 0\,14 \;\; b_1 \quad 0\,94 \;\; b_2 \quad 0\,41 \;\; c_1 \quad 0\,68 \;\; c_2 \quad 0\,56$$

As Hebe (6) is a large main-belt asteroid, its shape is close to that of a sphere due to the e ects of gravity. Although the derived cellinoid shape model is asymmetric, its axial ratios $a\ b$ 0 84, $c\ b$ 0 92 are close to that of a sphere if we set a a_1 a_2 b b_1 b_2 c c_1 c_2.

5.2. Iris (7)

As Iris (7) was not inverted from Hipparcos data by Cellino et al. (2009), we attempted to model it using the cellinoid shape model. There are totally 69 sparse Hipparcos datapoints, and the observed solar phase angles are distributed between 16 45 and 31 64 . The best-fitting period is P 7 11281h, which is close to the result obtained when using the Kaasalainen method (Kaasalainen et al., 2002; Ďurech et al., 2011; Hanuš et al., 2013). However, the Kaasalainen result is based on lightcurves observed between 1950 to 1993, which also includes Hipparcos data. It could be a mean estimate for the rotational period over this time frame and the result may be a ected by the di erent data sources. The cellinoid shape model was also used to derive a pole orientation of (20 47), with a longitude deviation of 4 and a latitude deviation of 32 to the result Pole_1(16 15) by Kaasalainen's method. Obtaining an accurate pole orientation requires more accurate sparse data and more data points. Nevertheless, the asymmetric shape of the cellinoid model performs better than the traditional ellipsoid model. More or less, the derived period and pole orientation only from 69 observed snapshots provides rough estimates of the physical properties of Iris (7).

5.3. Flora (8)

Flora (8) is another asteroid not inverted by Cellino et al. (2009). As such, we applied the cellinoid shape model to 56 snapshots of Flora (8) in the Hipparcos dataset. The solar phase angles are between 17 21 and 29 86 , with a mean value of 22 89 . The best-fitting period is P 12 81710h, with a best-fitting pole orientation of (347 18), as shown in Tab. 2. The pole solution is close to the result Pole_2 with the longitude deviation 12 and the latitude deviation 13 obtained via Kaasalainen's method (Torppa et al., 2003; Ďurech et al., 2011; Hanuš et al., 2013).

5.4. Eunomia (15)

There are 83 snapshots of Eunomia (15) in the Hipparcos dataset, which was observed at solar phase angles between 13 62 and 25 88 . The cellinoid shape model derived a rotational period of P 6 08277h and a pole orientation of (353 55). The best-fitting period is the same as that derived via Kaasalainen's method (Kaasalainen et al., 2002; Nathues et al., 2005; Hanuš et al., 2013) and Cellino's inversion method (Cellino et al., 2009). The pole orientation is also close to the value of the pole (3 67) derived via Kaasalainen's method, with a longitude deviation of 10 a latitude deviation of 12 . Moreover, the cellinoid shape model also obtains a second pole orientation (346 67) with six semi-axes of

$$a_1 \quad 1 \;\; a_2 \quad 0\,50 \;\; b_1 \quad 0\,68 \;\; b_2 \quad 0\,40 \;\; c_1 \quad 0\,56 \;\; c_2 \quad 0\,14$$

The deviations in both the longitude and latitude directions to the pole solution (347 64) derived by Cellino et al. (2009) are less than 3 . We computed similar axial ratios, $b\ a$ 0 72 $c\ a$ 0 47, which are close to the ratios $b\ a$ 0 70 $c\ a$ 0 55 of Cellino et al. Furthermore, the derived pole solution (353 55) from the cellinoid shape model is also confirmed by the pole result (352 58) obtained by Tanga et al. (2003).

5.5. Melpomene (18)

We apply the cellinoid shape model to 100 snapshots of Melpomene (18), where the observed solar phase angles are located in the interval from 15 23 to 27 26 . The best-fitting rotational period is P 11 57039h and the pole orientation is (188 40) with the six semi-axes as shown in Tab. 2. Cellino et al. (2009) could not derive the same parameters based on the traditional ellipsoid in their inversion method, and the information on this asteroid is not provided by Ďurech et al. (2010). Fortunately Warner et al. (2009) obtained a rotational period P 11 570h, which is same as the result from the cellinoid shape model.

5.6. Harmonia (40)

In total there are 103 observed data points for Harmonia (40) in the Hipparcos dataset. The solar phase angles are distributed from 18 23 to 26 96 . Based on the

cellinoid shape model, we derive two possible results. The first best-fitting result is for a rotational period of P 8 91081h and a pole orientation of (219 38); while the second best-fitting result is for a rotational period of P 8 91083h and a pole orientation of (36 31). The derived rotational period is close to that determined by Cellino et al. (2009) as the data sources employed in two methods are the same, i.e. Hipparcos data. However, the cellinoid shape model derived two pole orientations. The reverse direction (39 38) of the first pole (219 38) is close to the pole (24 31) inverted by Cellino et al. (2009), while the second pole (36 31) is close to the pole (22 31) derived via Kaasalainen's method (Hanuš et al., 2011, 2013). The cellinoid shape model requires data points with higher accuracy to obtain a refined pole orientation.

5.7. Nysa (44)

There are a total of 53 Hipparcos data points of Nysa (44), which were observed with solar phase angles between 20 61 and 28 44 . The cellinoid shape model derived a rotational period P 6 42140h that is very similar to the ones derived via Kaasalainen's method (Kaasalainen et al., 2002; Delbo' and Tanga, 2009) and Cellino's method (Cellino et al., 2009). Although the derived pole orientation (293 33) is different to the pole (99 58) determined via Kaasalainen's method, it is similar to the pole (298 36) obtained via Cellino's method with a longitude deviation of 5 and a latitude deviation of 3 . Moreover, as Nysa (44) likely has an irregular shape, the pole solution is di erent to the pole result (102 50) obtained by Tanga et al. (2003).

5.8. Dembowska (349)

We applied the cellinoid shape model to 92 sparse Hipparcos data points of Dembowska (349), which has a solar phase angle distributed between 13 88 and 21 23 . The derived best-fitting rotational period is P 4 69055h. However, there are two possible pole orientations. The first one is a pole (335 24) with six semi-axes of

$$a_1 \quad 1 \;\; a_2 \quad 0\,20 \;\; b_1 \quad 0\,59 \;\; b_2 \quad 0\,50 \;\; c_1 \quad 1\,00 \;\; c_2 \quad 0\,01$$

With a longitude deviation of 13 and a latitude deviation of 6 , the pole result is similar to the result (322 18) derived via Kaasalainen's method (Torppa et al., 2003;

Hanuš et al., 2013). The second pole orientation is (342 37) with six semi-axes of

$$a_1 \quad 1 \; a_2 \quad 0\,21 \; b_1 \quad 0\,59 \; b_2 \quad 0\,51 \; c_1 \quad 0\,98 \; c_2 \quad 0\,01$$

5.9. Eleonora (354)

There are a total of 98 snapshots of Eleonora (354) in the Hipparcos dataset, where the observed solar phase angle is distributed between 13 89 and 23 20 . The cellinoid shape model was applied to search for the best-fitting parameters to Eleonora (354). The best-fitting period is about P 4 28797h, which is close to the period obtained by Cellino et al. (2009). As previously mentioned, Cellino et al. exploited the same data source as considered here. However, the cellinoid shape model derived two possible pole orientations, (309 66) and (325 44). The reverse direction (145 44) of the second pole solution (325 44) is similar to the pole solution (144 54) derived via Kaasalainen's method (Hanuš et al., 2011, 2013), with a longitude deviation of 1 and a latitude deviation of 10 .

5.10. Papagena (471)

There are a total of 112 snapshots of Papagena (471) in the Hipparcos dataset. The cellinoid shape model derived a rotational period of P 7 11534h and a pole orientation of (217 40). The period is almost same as the result P 7 115394h derived via Kaasalainen's method (Ďurech et al., 2011). The longitude deviation of the two pole results derived by the two di erent methods is 6 , with a latitude deviation of 27 .

Table 2 shows all the best-fitting solutions derived by the cellinoid shape model for the 11 asteroids recorded by Hipparcos. Generally the cellinoid shape model can derive reasonable estimates from the sparse photometric data due to its asymmetric and easily representative shape. Encouragingly, it derives rotational periods that are close to those determined by other authors. The cellinoid shape model is able to search for the best-fitting value of the pole and provide best estimates of pole orientations better than the ellipsoid shape model. Moreover, the cellinoid shape model can also derive reasonable solutions to the asteroids, such as Iris (7), Flora (8), and Melpomene (18),

which were not modelled by the inversion methods that were based on the ellipsoid shape model.

As the Hipparcos data are not accurate, in which there are many observed points with photometric errors greater than 0 05 mag, the derived solutions obtained via the cellinoid shape model may di er from the results derived from the modelling of lightcurves performed in Kaasalainen's method. Nevertheless, the cellinoid shape model can be employed to derive the rough estimates for a given asteroid from sparse photometric data instead of via the traditional triaxial ellipsoid approach. Our examples confirm that the cellinoid shape model can not only derive the rotational period, but also derive better estimates of pole orientations compared with the ellipsoid model.

6. Conclusions and Future Work

In this article, we presented the cellinoid shape model that is used for deriving physical parameters of some asteroids from the sparse Hipparcos datseta. Following the error analysis and the technique, which makes the algorithm more stable and efficient, the e ectiveness of cellinoid shape model is confirmed from modelling of the simulated sparse data. Finally the cellinoid shape model was employed to search for the best-fitting parameters for specific asteroids in the Hipparcos dataset, and the computed parameters were compared with the known results via Kaasalainen's method and Cellino's inversion solutions in Table 2. According to the preliminary results shown in this paper, we can say that the cellinoid shape model can fit the asteroids better than the ellipsoid model, and the derived parameters from sparse data are close to the ones derived from Kaasalainen's approach. In the future, as Gaia sparse data for asteroids become available, the cellinoid shape model will be applied to estimate the physical parameters in an e cient way for the likely huge number of observed asteroids.

In conclusion, the cellinoid shape model seems to be, not unexpectedly, better than the traditional triaxial ellipsoid model, which was confirmed both theoretically and numerically. As far as limited datasets are concerned, the cellinoid shape model can be applied to e ciently determine estimates of the physical parameters of a given asteroid. If the data sources are multiple or the collected lightcurves are sampled well enough,

Kaasalainen's method can be applied to refine the shapes and the parameters of the modelled asteroid.

As the cellinoid shape model consists of eight octants of ellipsoids, in future work we want to find a theoretical formula to directly calculate the brightness since this would reduce enormously the necessary CPU time, and would make the cellinoid shape model more suited to be systematically adopted for the inversion of big sets of photometric data. Moreover, if a feasible formula could provide an initial estimate of the period and pole, it would save a considerable amount of time when deriving the best-fitting parameters via the cellinoid shape model presented in this article. This is valuable in the case of estimating the parameters for large numbers of asteroids with limited sparse photometric dataset, such as those observed by space satellites.

Acknowledgements

This work is funded under the grant NO. 095 2013 A3 and 039 2013 A2 from the Science and Technology Development Fund, MSAR. W.-H. Ip is supported by MSAR Science and Technology Fund (Project No. 019 2010 A2) and NSC 101-2111-M-008-016. And we sincerely thank the anonymous reviewers for their professional and constructive comments.

References

References

Cellino, A., Dell'Oro, A., 2012. The derivation of asteroid physical properties from gaia observations. Planetary and Space Science 73, 52 – 55. Solar System science before and after Gaia.

Cellino, A., Hestro er, D., Tanga, P., Mottola, S., Dell'Oro, A., 2009. Genetic inversion of sparse disk-integrated photometric data of asteroids: application to Hipparcos data. A&A 506, 935–954.

Cellino, A., Zappalà, V., Farinella, P., 1989. Asteroid shapes and lightcurve morphology. Icarus 78, 298–310.

Delbo', M., Tanga, P., 2009. Thermal inertia of main belt asteroids smaller than 100 km from IRAS data. Planetary and Space Science 57, 259–265.

Drummond, J.D., Conrad, A., Merline, W.J., Carry, B., Chapman, C.R., Weaver, H.a., Tamblyn, P.M., Christou, J.C., Dumas, C., 2010. Physical Properties of the ESA Rosetta target asteroid (21) Lutetia I. The triaxial ellipsoid dimensions, rotational pole, and bulk density. A&A 523, A93.

Hanuš, J., Marchis, F., Ďurech, J., 2013. Sizes of main-belt asteroids by combining shape models and Keck adaptive optics observations. Icarus 226, 1045–1057.

Hanuš, J., Ďurech, J., Brož, M., Warner, B.D., Pilcher, F., Stephens, R., Oey, J., Bernasconi, L., Casulli, S., Behrend, R., Polishook, D., Henych, T., Lehký, M., Yoshida, F., Ito, T., 2011. A study of asteroid pole-latitude distribution based on an extended set of shape models derived by the lightcurve inversion method. A&A 530, A134.

Hestro er, D., Morando, B., Hog, E.and Kovalevsky, J., Lindegren, L., Mignard, F., 1998. The HIPPARCOS solar system objects catalogues. A&A 334.

Jordi, C., Gebran, M., Carrasco, J.M., de Bruijne, J., Voss, H., Fabricius, C., Knude, J., Vallenari, A., Kohley, R., Mora, A., 2010. Gaia broad band photometry. A&A 523, 1–16.

Kaasalainen, M., Lamberg, L., 1992a. Interpretation of lightcurves of atmosphereless bodies. I-General theory and new inversion schemes. A&A 259, 318–332.

Kaasalainen, M., Lamberg, L., 1992b. Interpretation of lightcurves of atmosphereless bodies. II-Practical aspects of inversion. A&A 259, 333–340.

Kaasalainen, M., Lu, X.P., Vänttinen, A., 2012. Optimal computation of brightness integrals parametrized on the unit sphere. A&A 539.

Kaasalainen, M., Torppa, J., 2001. Optimization Methods for Asteroid Lightcurve Inversion I. Shape Determination. Icarus 153, 24–36.

Kaasalainen, M., Torppa, J., Muinonen, K., 2001. Optimization Methods for Asteroid Lightcurve Inversion II. The Complete Inverse Problem. Icarus 153, 37–51.

Kaasalainen, M., Torppa, J., Piironen, J., 2002. Models of twenty asteroids from photometric data. Icarus 159, 369 – 395.

Kaasalainen, S., Kaasalainen, M., Piironen, J., 2005. Ground reference for space remote sensing Laboratory photometry of an asteroid model. A&A 440, 1177–1182.

Karttunen, H., 1989. Modelling asteroid brightness variations. I-Numerical methods. A&A 208, 314–319.

Karttunen, H., Bowell, E., 1989. Modelling asteroid brightness variations. II-The interpretability of light curves and phase curves. A&A 208, 320–326.

Lu, X.P., Ip, W.H., 2015. Cellinoid shape model for multiple light curves. Planetary and Space Science 108, 31–40.

Lu, X.P., Zhao, H., You, Z., 2013. A Fast Ellipsoid Model for Asteroids Inverted From Lightcurves. Research in Astronomy and Astronphysics 13, 465–472.

Lu, X.P., Zhao, H., You, Z., 2014. Cellinoid Shape Model for Asteroids. Earth, Moon and Planets 112, 73–87.

Muinonen, K., Piironen, J., Kaasalainen, S., Cellino, A., 2002. Asteroid photometric and polarimetric phase curves: Empirical modeling. Memorie Della Società Astronomica Italiana 73, 716–719.

Nathues, A., Mottola, S., Kaasalainen, M., Neukum, G., 2005. Spectral study of the eunomia asteroid family: I. eunomia. Icarus 175, 452 – 463.

Ohba, Y., Abe, M., Hasegawa, S., Ishiguro, M., Kwiatkowski, T., Colas, F., Dermawan, B., Fujiwara, A., 2003. Pole orientation and triaxial ellipsoid shape of (25143) 1998 SF36, a target asteroid of the MUSES-C mission. Earth, Planets and Space 55, 341–347.

Perryman, M.A.C., Lindegren, L., Kovalevsky, J., Hoeg, E., Bastian, U., Bernacca, P., et al., 1997. The HIPPARCOS Catalogue. A&A 323.

Santana-Ros, T., Bartczak, P., Michałowski, T., Tanga, P., Cellino, A., 2015. Testing the inversion of asteroids' gaia photometry combined with ground-based observations. Monthly Notices of the Royal Astronomical Society 450, 333–341.

Surdej, A., Surdej, J., 1978. Asteroid lightcurves simulated by the rotation of a three-axes ellipsoid model. A&A 66, 31–36.

Tanga, P., Hestro er, D., Cellino, A., Lattanzi, M., Martino, M., Zappalà, V., 2003. Asteroid Observations with the Hubble Space Telescope FGS II. Duplicity search and size measurements for 6 asteroids. A&A 401, 733–741.

Torppa, J., Kaasalainen, M., Michałowski, T., Kwiatkowski, T., Kryszczyńska, A., Denchev, P., Kowalski, R., 2003. Shapes and rotational properties of thirty asteroids from photometric data. Icarus 164, 346 – 383.

Ďurech, J., Kaasalainen, M., Herald, D., Dunham, D., Timerson, B., Hanuš, J., Frappa, E., Talbot, J., Hayamizu, T., Warner, B.D., Pilcher, F., Galád, A., 2011. Combining asteroid models derived by lightcurve inversion with asteroidal occultation silhouettes. Icarus 214, 652 – 670.

Ďurech, J., Sidorin, V., Kaasalainen, M., 2010. DAMIT: a database of asteroid models. A&A 513, 46.

Warner, B.D., Harris, A.W., Pravec, P., 2009. The asteroid lightcurve database. Icarus 202, 134 – 146.

(a)

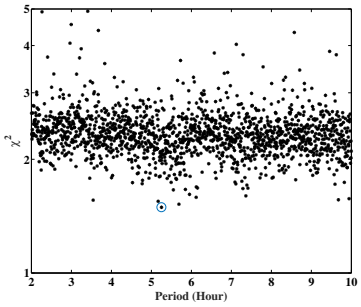

(b)

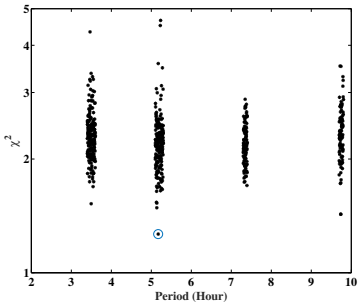

(c)

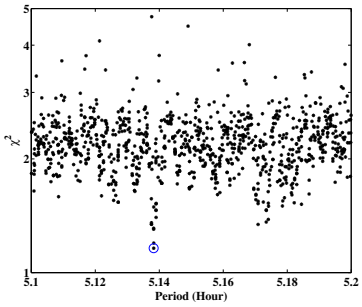

Figure 6: Searching for the best-fitting period (circled point) from Hipparcos data of Laetitia (39). (a) searching the interval [2,10] with P 0 005h; (b) searching the interval [3.4 - 3.6, 5.1 - 5.3, 7.3 - 7.4, 9.7 - 9.8] with P 0 001h; (c) searching the interval [5.1, 5.2] with P 0 0001h

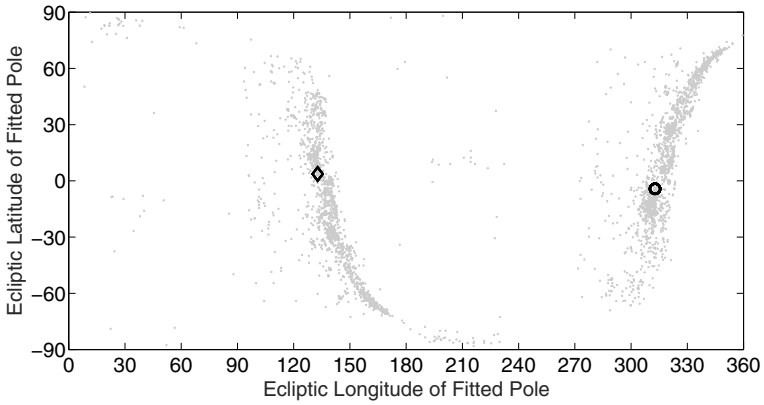

Figure 7: Searching for the best-fitting pole orientation (big circle) and accompanying solution (big diamond) from Hipparcos data of Laetitia (39).

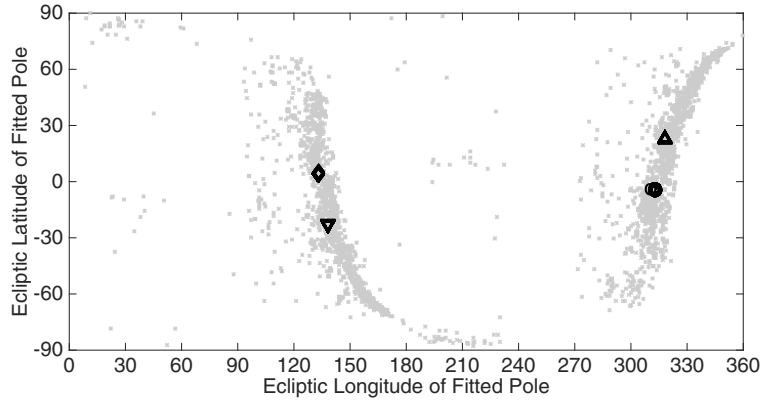

Figure 8: Two groups of the best-fitting pole orientation of Laetitia (39).

Table 2: Comparison of known parameters of 11 asteroids derived from di erent methods

NO.	DAMIT	Cellino et al.(2009)	Cellinoid Models
Hebe(6) N 91	P_1 7 274471 h, P_2 7 274470 h, Pole$_1$ (340 42), Pole$_2$ (345 42)	P_1 7 27290 h, P_2 7 27275 h, Pole$_1$ (45 75), Pole$_2$ (93 37), (295 29)	P 7 27806 h, Pole (342 39), [1 0 14 0 94 0 41 0 68 0 56]
Iris(7) N 69	P 7 138843 h, Pole$_1$ (16 15), Pole$_2$ (196 2)	Not Inverted	P 7 11281 h, Pole (20 47), [1 0 08 0 46 0 33 0 22 0 21]
Flora(8) N 56	P 12 86667 h, Pole$_1$ (155 6), Pole$_2$ (335 5)	Not Inverted	P 12 81710 h, Pole (347 18), [1 0 10 0 80 0 25 0 75 0 30]
Eunomia(15) N 83	P 6 082753 h, Pole (3 67)	P 6 08273 h, Pole (347 64)	P 6 08277 h, Pole$_1$ (353 55), [1 0 46 0 66 0 30 0 70 0 25] Pole$_2$ (346 67), [1 0 50 0 68 0 40 0 56 0 14]
Melpomene(18) N 100	Not Provided	Not Inverted	P 11 57039 h, Pole (188 40), [1 0 23 0 85 0 55 0 64 0 63]
Laetitia(39) N 112	P 5 138238 h, Pole (323 32)	P 5 13830 h, Pole$_1$(335 47), Pole$_2$(126 20)	P_1 5 13830 h, Pole$_1$ (313 4), [1 0 65 0 74 0 43 0 62 0 43] P_2 5 13827 h, Pole$_2$ (318 23), [1 0 61 0 67 0 51 0 57 0 45]
Harmonia(40) N 103	P 8 908483 h, Pole (22 31)	P 8 91069 h, Pole (24 31)	P_1 8 91081 h, Pole$_1$ (219 38), [1 0 01 0 81 0 13 0 47 0 47] P_2 8 91083 h, Pole$_2$ (36 31), [1 0 02 0 81 0 12 0 47 0 46]
Nysa(44) N 53	P 6 421417 h, Pole (99 58)	P 6 42160 h, Pole (298 36)	P 6 42140 h, Pole (293 33), [1 0 70 0 81 0 25 0 72 0 29]
Dembowska(349) N 92	P 4 701204 h, Pole (322 18),	P_1 4 69120h, P_2 4 70153 h, Pole$_1$ (201 71), Pole$_2$ (137 11)	P 4 69055 h, Pole$_1$ (335 24), [1 0 20 0 59 0 50 1 00 0 01] Pole$_2$ (342 37), [1 0 21 0 59 0 51 0 98 0 01]
Eleonora(354) N 98	P 4 277186 h, Pole (144 54)	P 4 28972 h, Pole (335 15)	P_1 4.28797 h, Pole$_1$ (309 66), [1 0 30 0 61 0 40 0 38 0 09] P_2 4.28798 h, Pole$_2$ (325 44), [1 0 01 0 96 0 02 0 97 0 63]
Papagena(471) N 112	P 7 115394 h, Pole (223 67)	P 7 10540 h, Pole (246 74)	P 7 11534 h, Pole (217 40), [1 0 44 0 72 0 48 0 84 0 06]

Highlights

* Cellinoid Shape Model Consisting of Eight Octants From Eight Ellipsoids
* Search Physical Parameters of Asteroids from Sparse Photometric Data
* Error Propagation, Simulated Numerical Test and Hipparcos Data